



ML-Tree and MRL-Tree: Combining Mass-Spring System, Rigid-Body Dynamics and L-Systems to Model Physical Effects on Trees

See Min Lim¹ ^a and Like Gobeawan² ^b

¹National University of Singapore, 21 Lower Kent Ridge Road, Singapore

²Institute of High Performance Computing (IHPC), Agency for Science, Technology and Research (A*STAR),
1 Fusionopolis Way #16-16 Connexis, 138632, Singapore

Keywords: Physically-Based Modeling, Tree Modeling, Root Modeling, L-Systems, MSS, RBD.

Abstract: We apply physically-based modeling methods to a biological tree model for a hybrid model with a better accuracy. Physical aspects of tree growth, such as wind, tropisms, gravity and soil resistance are modelled. The hybrid model also includes the handling of boundary conditions such as momentum conservation and switching between the L-System, Mass-Spring System (MSS) and Rigid-Body Dynamics (RBD) methods. This paper demonstrates resulting models and their potential applications such as tree stress prediction.

1 INTRODUCTION

Trees and other greeneries are planted at urban areas to provide shade and to reduce temperatures (Wong et al., 2021). Along with that, they may cause safety hazards due to uprooting and falling branches. They can be managed through measures like tree health assessment and tree pruning.

Given the increasing prominence of digital twin cities (Ballouch et al., 2022) (Tao et al., 2022) (Pomeroy, 2023), there are great potentials for digital twin trees through an automated large-scale tree management system such as (Gobeawan et al., 2021a) (Gobeawan et al., 2018) to consider biological growth rules and mechanical responses to the environment. Such digital twin trees can be utilised to predict tree branch stress and uprooting.

2 RELATED WORK

Some existing L-System-based tree modelling techniques (Gobeawan et al., 2021b) (Yi et al., 2018) (Stava et al., 2014) focus on implementing tree growth processes without accounting for the tree tropisms, which are tree growth responses to environment stimuli. Accounting for such responses will allow for more accurate tree models in urban contexts of


intertwining environment components, hence a better urban planning. (Moulton et al., 2020) and (Hädrich et al., 2017) account for tree growth responses as mechanical responses by modelling tree stems as inextensible elastic rods and particles, respectively. However, neither of them integrates the domain knowledge of botanical growth processes such as branching patterns. (Jirasek et al., 2000) is similar, but it is L-System-based (Prusinkiewicz and Lindenmayer, 1990) thus allowing for some biological considerations. However it does not consider interactions between parent and child branches.

Our previous work (Lim and Gobeawan, 2023) combines Mass-Spring System (MSS) and L-Systems to generate biologically- and physically-plausible tree models. This current work will provide crucial implementation details and results, as well as discuss new work on root modeling and including Rigid-Body Dynamics (RBD).

3 METHODS

Our tree models were generated based on (Gobeawan et al., 2021b) where stems were built by producing new node-and-internode pairs at the buds based on L-System growth rules over time. During the growth process, we concurrently built a MSS into our tree models to model mechanical responses for our first model of Mass-Spring L-Systems (henceforth de-

^a  <https://orcid.org/0009-0008-0576-556X>

^b  <https://orcid.org/0000-0001-6501-6394>

noted as ML-Tree). For our second Mass-Spring L-Systems with RBD model (denoted as MRL-Tree), we further added RBD to model older portions of the tree.

With these models, we considered tropisms (phototropism and gravitropism), weight of the tree nodes, roots and soil resistance. Stress prediction and automatic branch-breaking were also tested in the former model.

Our images and models were generating using L-Py and PlantGL (Boudon et al., 2012).

3.1 Mass-Spring L-System (ML-Tree)

When incorporating the MSS (Witkin et al., 2001) onto the L-System layer, we consider the nodes to be point masses while the internodes were springs. The algorithm is described in the following pseudocode:

```

initialization;
for number of age timesteps do
  tree grows for 1 unit of age by L-System
  production rules;
  for number of substeps do
    calculate forces acting on each MSS
    node;
    calculate and update new position of
    each node;
  end
end

```

Algorithm 1: ML-Tree.

Firstly, we initialised expandable matrices to keep track of nodal information and spring connection information. We also set the growth and physical variables (such as the trunk height and wind speed) to specific values or as functions. The tree then grows for one unit of age by L-System production rules, where one unit of age is the time needed to grow one node-and-internode pair at each bud. This is the smallest unit of growth possible in our model, chosen to minimise the time lag between the growth and the applying of forces. We then added the new node(s) grown, their corresponding nodal information and the new spring(s) information to the bookkeeping matrices. Internal forces acting on each node (such as the spring forces) are calculated based on the MSS model. Other external forces acting on the nodes (such as gravity and tropisms) are also calculated and added, and new positions after the substep are found. This force and position calculation is then repeated for the number of substeps. This tree growth and force-and-position calculation then repeats until the tree has reached its specified age.

3.1.1 Conserving Momentum

In our model, the total and individual masses regularly increases, hence the law of conservation of linear momentum must be considered.

During the growth process, when a new node j is grown, it shares the original linear momentum, $m_i^t v_i^t$, of the node i which it grew from. Nodes i and j have the same new velocity, $v^{t+\delta t}$, since forces are not considered during this growth stage. To simplify calculations, we assume that new nodes are grown instantaneously at the start of the growth process, thus the mass for the older node i at times t and $t + \delta t$ are considered the same. We calculate the new velocities of nodes i and j through Equation 1. $m_j^{t+\delta t}$ is the smallest mass a new node can have in our model.

$$v_j^{t+\delta t} = v_i^{t+\delta t} = \frac{m_i^t v_i^t}{m_i^{t+\delta t} + m_j^{t+\delta t}} \quad (1)$$

At the end of each age timestep, the mass of the nodes are recalculated by multiplying the new volume of their internodes with the wood density. The velocity of nodes are re-calculated by dividing the original linear momentum with the new mass.

3.1.2 Spring Constants and Angle Springs

The spring constant of each spring are directly proportional to the diameter d of the internode and inversely proportional to the internode's rest length l (Smith, 2010). The values of the spring constants were roughly based on the spring constants of wood in (Russell and Hunt, 2009). Nodes which have reached a certain wooden age are considered to be woody and will have a stiffer base spring constant k_0 .

$$k = \frac{k_0 d}{l} \quad (2)$$

Secondary (angle) springs were added between alternate nodes to control angles, similar to (Van Haevre et al., 2006). We used the same Equation 2 to find the secondary spring constants, and we did not differentiate between the spring types for k_0 .

3.1.3 Implicit Method Equations

We used an implicit Euler method (or backward Euler) for integration in our MSS. We tested two equations to estimate Δv_i^{t+h} , Equation 3 (Kang et al., 2001) and Equation 4 (Kang et al., 2000) (Mesit et al., 2007). \tilde{F}_i^t is the sum of all forces acting on node i at time t , and its unit vector is \hat{F}_i^t .

$$\Delta \mathbf{v}_i^{t+h} = \frac{\bar{\mathbf{F}}_i^t h + h^2 \sum_{(i,j) \in E} k_{ij} \bar{\mathbf{F}}_j^t h / (m_j + h^2 \sum_{(j,k) \in E} k_{jk})}{m_i + h^2 \sum_{(i,j) \in E} k_{ij}} \quad (3)$$

$$\Delta \mathbf{v}_i^{t+h} = \frac{\bar{\mathbf{F}}_i^t h + h^2 \sum_{(i,j) \in E} k_{ij} |\Delta \mathbf{v}_j^t| \bar{\mathbf{F}}_j^t}{m_i + h^2 \sum_{(i,j) \in E} k_{ij}} \quad (4)$$

These implicit methods required artificial damping for stability, which is given by Equation 5 in our model.

$$\mathbf{F}_{damping} = c \sqrt{k(m_1 + m_2)} (\mathbf{v}_j - \mathbf{v}_i) \quad (5)$$

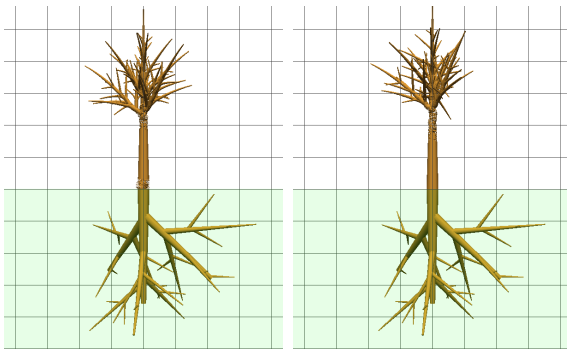
It is chosen to be proportional to $\sqrt{k(m_1 + m_2)}$ to account for changing masses and spring constants since we are modeling a growing tree. This coefficient is based on the formula for the critical damping coefficient, although we note that this Equation 5 is not always able to achieve stability across all portions of the tree.



(a) Equation 3.

(b) Equation 4.

Figure 1: Comparison of the ML-Tree model using Equation 3 and 4.



(a) Equation 3.

(b) Equation 4.

Figure 2: Another comparison of the model using Equations 3 and 4.

Figure 1 attains a stable configuration of damping and spring constants for using Equation 3, and it is

compared with how Equation 4 perform for the same set of variables. We tried to achieve the opposite situation in Figure 2, but we see that Equation 3 is similarly realistic. Equation 3 tended to produce largely realistic and stable models over a range of damping and spring constants, while Equation 4 was only stable and realistic across a much narrower range.

3.2 Mass-Spring L-System with RBD (MRL-Tree)

Our second model adds RBD (Baraff, 2001) (Pedersen, 2003) onto the existing MRL-Tree model. This is described in algorithm 2. We used quaternions (Betsch and Siebert, 2009) for the rotation and a 4-th order Runge-Kutta (Pedersen, 2003) to solve the differential equations.

```

initialization;
for number of age timesteps do
  tree grows for 1 unit of age by L-System
  production rules;
  add nodes which have reached a specified
  rigid age to the Rigid-Body (RB)
  system;
  for number of substeps do
    calculate forces acting on each RB
    node;
    calculate and update new position of
    each RB node;

    calculate forces acting on each MSS
    node;
    calculate and update new position of
    each MSS node;
  end
end

```

Algorithm 2: MRL-Tree.

Our algorithm for this MRL-Tree model is similar to that for the first model, except that the forces and positions of the RB nodes are considered first before that of the MSS nodes during each substep.

3.2.1 Handling Boundary Conditions for RBD

When a node reaches a specified age, it is considered to have hardened and is added to the RB system. In this subsection, t is at the end of the L-System stage and $t + \delta t$ is after the checking of age and assignment to the RB system, at the start of the first substep. Nodes j are these new RB nodes while nodes i are existing RB nodes.

The centre of mass of the RB system \mathbf{x} and the system's linear momentum \mathbf{p} can be directly calculated through Equations 6 and 7. M is the sum of mass of the RB system. However since the RB system is constantly increasing in size, the centre of mass does not have a constant position relative to other positions in the RB system, therefore its original angular momentum L^t is not conserved. Hence, we hypothesise that in Equation 8, an extra term $\Sigma(\mathbf{x}_{\Delta i}^{t+\delta t} \times m_i^t \mathbf{v}_i^t)$ should be added to account for any change in angular momentum due to the changing position of the centre of mass. In Equation 8, $\mathbf{x}_{\Delta i}^{t+\delta t}$ refers to the relative position of node i at time t (or $t + \delta t$), to the centre of mass at time $t + \delta t$; in other words, $\mathbf{x}_{\Delta i}^{t+\delta t} = \mathbf{x}_i^t - \mathbf{x}^{t+\delta t}$.

$$\mathbf{x}^{t+\delta t} = \frac{\Sigma m_i^t \mathbf{x}_i^t + \Sigma m_j^t \mathbf{x}_j^t}{M^{t+\delta t}} \quad (6)$$

$$\mathbf{p}^{t+\delta t} = \mathbf{p}^t + \Sigma m_j^t \mathbf{u}_j^t \quad (7)$$

$$\begin{aligned} L^{t+\delta t} \approx & L^t + \Sigma(\mathbf{x}_{\Delta j}^{t+\delta t} \times m_j^t \mathbf{v}_j^t) \\ & + \Sigma(\mathbf{x}_{\Delta i}^{t+\delta t} \times m_i^t \mathbf{v}_i^t) \end{aligned} \quad (8)$$

3.3 Gravity, Phototropism, Gravitropism, Wind and Air Viscosity

Gravity, F_g , was calculated by multiplying the node's mass with \mathbf{g} , the acceleration due to gravity on Earth.

Phototropism refers to the plant's reorientation towards light source and we modelled it with a $F_{phototropism}$ which pulls the buds towards a specified point of light (Moulton et al., 2020). Its magnitude is a constant multiplied by the intensity of the light. The light intensity is inversely proportional to the square of the distance between the bud and the light source. In future work, auxins should be considered to improve accuracy (Zhou et al., 2017).

Gravitropism is the response of a plant to gravity. Generally, the plant reorientates itself against the direction of gravity and we modelled this $F_{gravitropism}$ based on the sine law method (Dumais, 2013). It is applied on all nodes except the buds.

Wind was modelled using Equation 10, using a general wind load formula. The constant in Equation 9 is only applicable for metric system of units, and 0.00256 should be used for the imperial system of units. A is the area of the object for which we took the cross-sectional area of the node, P is the wind pressure and C_{drag} is the drag coefficient (set to 1 in our model (Suzuki and Arikawa, 2010)).

$$P = 0.613 |v_{wind}|^2 \quad (9)$$

$$\mathbf{F}_{wind} = (A \times P \times C_{drag}) \hat{\mathbf{d}}_{wind} \quad (10)$$

Air viscosity was modelled based on Stokes' Law (Equation 11). In our model, η is the fluid viscosity (1.81×10^{-5} for air), R is the radius of the node and v is the velocity of the node.

$$\mathbf{F}_{drag} = 6\pi\eta Rv \quad (11)$$

3.4 Roots and Soil Resistance

There is currently a lack of research on root architecture and modeling (Harahap et al., 2018)(Alani and Lantini, 2020), especially those using a compatible L-System method or for trees. This is partly due to the difficulty in collecting underground root data, though there has been recent advances in non-destructive root testing methods (Alani and Lantini, 2020) (Atkinson et al., 2019). Since any future biological modeling of tree roots can be added retrospectively into our model, we decided to focus on modeling the mechanical reactions of roots, and we modified the above-ground tree growth to create a tentative model for the roots (Figure 3).

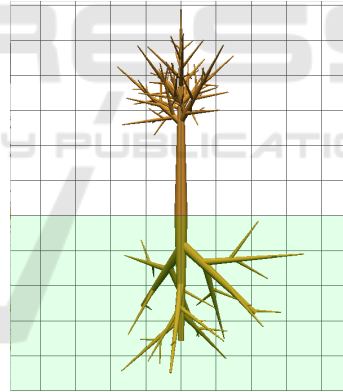


Figure 3: Tree model with roots, without mechanical forces.

To add soil resistance, we tested two models based on (Pang et al., 2023) and (Imhoff et al., 2016). For quantitative data on the soil (such as clay content or organic matter content), we referred to (Rezaur et al., 2003). Since the nodes underground are almost completely surrounded by the soil, we consider that the roots can counter a net force in every direction. The soil resistance calculated is considered to be the maximum soil resistance for the node.

The first method uses Equation 12 (Pang et al., 2023) and bulk density values from (Rezaur et al., 2003). The poisson's ratios used were estimated based on the water content. γ is the soil density, μ

is Poisson's ratio, P_a is the remaining pressure, r is the radius of the cone and h is the penetration depth.

$$B = \left(\frac{\gamma}{1000}\right)^{12} \times (0.5 - \mu)^{\frac{1}{3}} / 2.8$$

$$|F_{max}| = \left(\frac{P_a}{10000} \times \frac{\gamma \times 9.8}{1000000} \times \frac{2}{3} \pi \times r^3\right)^{\frac{1}{2}} \times h \times 100 \times B \quad (12)$$

The second method uses Equation 14 from (Imhoff et al., 2016) and soil data values from (Rezaur et al., 2003). SR is the soil resistance to penetration in MPa . $clay$ represents the percentage clay content while OM represents the percentage organic matter content. θ is the volumetric water content, BD is the bulk density of soil and A is the surface area. The coefficients c_0 , c_1 , c_2 , d_0 , d_1 and e_0 are given in (Imhoff et al., 2016).

$$\ln SR = c_0 + c_1 clay + c_2 OM + (d_0 + d_1 clay) \ln \theta + e_0 \ln BD \quad (13)$$

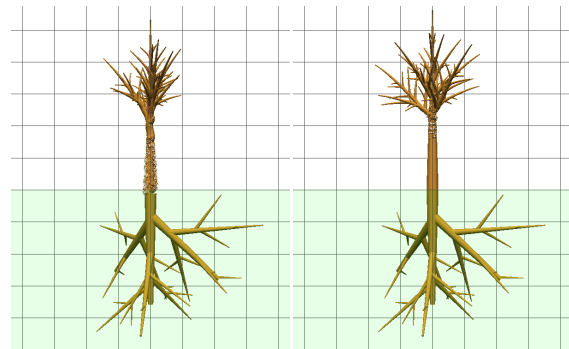
$$|F_{max}| = 1000000 \times SR \times A \quad (14)$$

Figures 4, 5 and 6 show both methods using soil data from three different locations (Yishun, Mandai and NTU) in Singapore, with only gravity applied. We notice some instability in almost all the cases, which could be due to a number of reasons. Firstly, our model is not an accurate representation of root structure as discussed above. Secondly, it does not consider soil penetration during root growth, including any changes to the root model and soil profile as a result. Furthermore, our model also does not include collision detection as this would be too computationally costly.

Overall, we consider the second method to be more suitable. This is because it allows direct alteration in the soil type since the percentages of clay, water, bulk density, organic matter are all considered. We also notice that for the Yishun tree models, the second method is mostly stable, unlike for the first method. Both models are unstable for the Mandai and NTU models.

3.5 Stress Prediction and Automatic Branch-Breaking

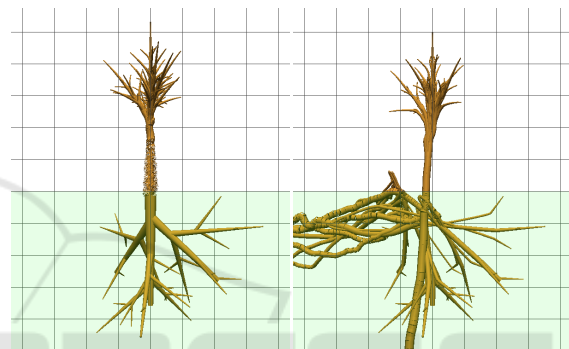
Given that our ML-Tree model keeps track of forces and nodal information, we can calculate and predict the stress on each node. This is shown in Figure 7. The colour varies on a logarithmic scale; darker blue indicates more stress and the lightest blue appears nearly white.



(a) Method 1.

(b) Method 2.

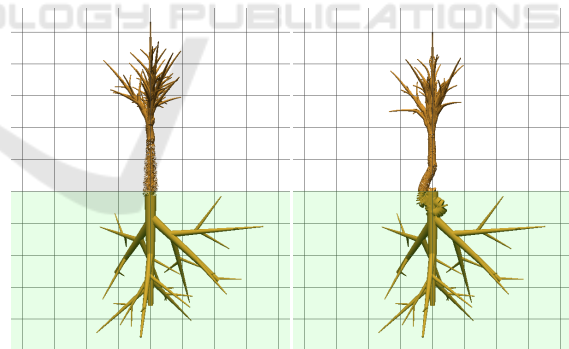
Figure 4: Comparison using Yishun's environment.



(a) Method 1.

(b) Method 2.

Figure 5: Comparison using Mandai's environment.



(a) Method 1.

(b) Method 2.

Figure 6: Comparison using NTU's environment.

Based on the stress, we can also set an automatic branch breaking limit. This can help improve our digital twin tree model accuracy by automatically removing branches experiencing a high level of stress, which would have naturally fallen.

From Figure 7, the areas under most stress (e.g. when the branches curve downwards significantly), are darkly coloured as expected. However, from Figure 7, the sudden changes in colour of neighbouring

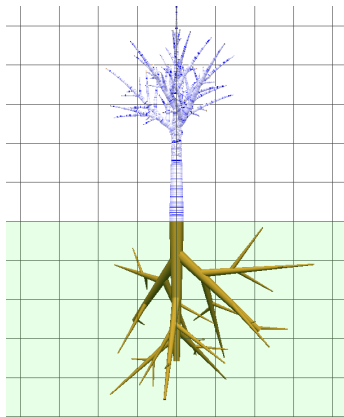


Figure 7: Tree model coloured based on stress.

internodes suggests that our models have difficulty reaching a final equilibrium state.

4 RESULTS AND DISCUSSION

In this section, we compared the two models. Our examples were generated based on a 25 year-old *Hopea odorata* tree. The age when nodes become rigid was set to 3 years for the MRL-Tree model.

4.1 Gravity

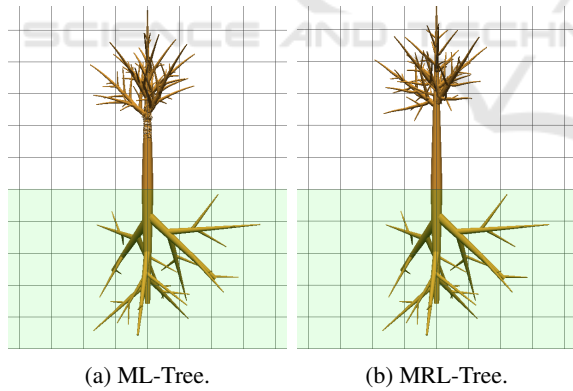


Figure 8: Comparison of gravity effects on the two models.

We noticed from Figure 8 that MRL-Tree model was significantly more rigid than our ML-Tree model.

4.2 Tropisms

Figure 9 shows a comparison of the two models with phototropism applied, and the trees can be seen bending towards the light source on the right. Figure 10 has gravitropism applied, and the tree branches are seen bending upwards as expected. We noticed that

the two models produced essentially identical results in both cases.

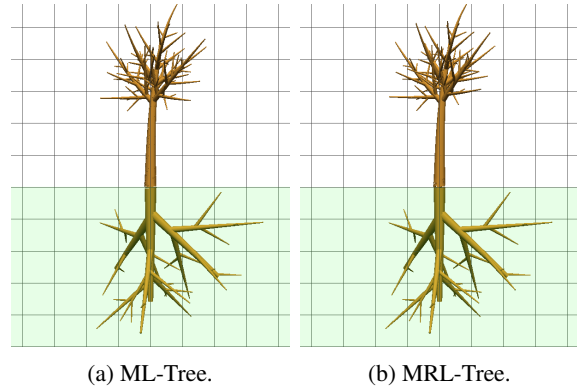


Figure 9: Comparison of phototropism effects on the two models.

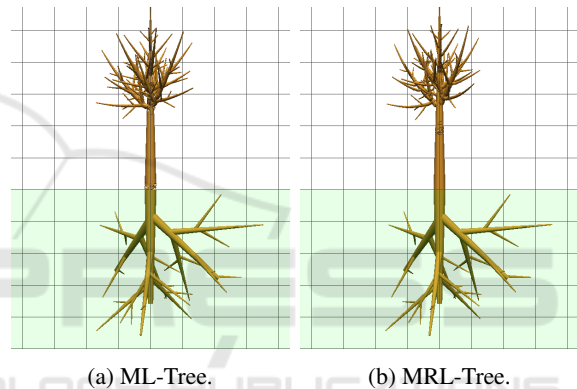


Figure 10: Comparison of gravitropism effects on the two models.

4.3 Wind

We also tested adding wind to our model, as shown in Figure 11. However, for our ML-Tree model, the elasticity and difficulty in propagation of forces causes our tree to collapse. Since we did not implement the tree collapse processes, Figure 11a appears unstable. This is not the case in our MRL-Tree model, which compels the forces to be completely propagated.

4.4 Comparison of the Two Models

From the model with wind applied (Figure 11), we see that the soil resistance has difficulty keeping the ML-Tree upright, causing the instability. This is because the ML-Tree model has difficulty propagating the forces throughout the system within its 50 sub-steps per L-System time-step, resulting in the model appearing to be too elastic. Meanwhile the MRL-Tree calculates the displacement effects for the whole RB system together, compelling the forces to be propa-

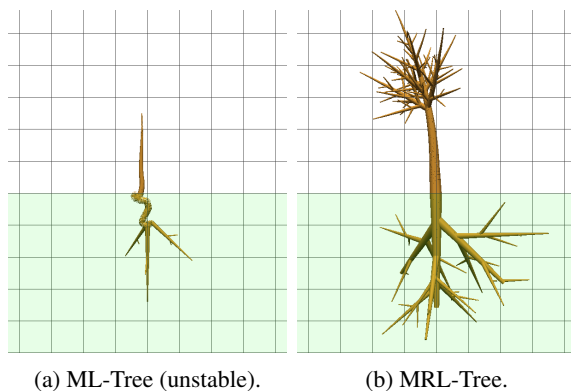


Figure 11: Comparison of wind effects on the two models.

gated, and therefore it is more stable and realistic.

However, this second model also faces stiffness issues as seen from the case with gravity (Figure 8). Furthermore, stress prediction and automatic branch breaking, as they are currently implemented, will not work with this second model since the RB nodes are not considered individually.

5 CONCLUSION

We have demonstrated the feasibility of applying physically-based methods to biological tree models to attain two plausible models which can predict crucial tree management information such as the relative amounts of stress acting on each node. Our models can be scaled to include other environmental and growth factors or to improve the current methods, as long as these factors can be modelled as forces. We also tested and compared varying methods of modeling soil resistance, of implicit integration and of predicting branch breaking possibility. In addition, we also detailed the methods we used to handle boundary conditions for both the ML-Tree model and the MRL-Tree model. Our models are largely built using existing real-life data and physical laws of nature, therefore they have the potential to be deployed for tree management, with integration with a large-scale tree-management system in a digital twin city.

However, our models currently suffer from stability issues. Furthermore, for the total duration of substeps and age timesteps to be equal, the substeps of the MSS will need be very large, or the model will be very computationally costly. More work can be done to further improve stability and accuracy or create a more accurate model to replace the tentative models currently used for roots. Other methods for solving ordinary differential equations can be explored to improve stability. The models can also benefit from

modeling more physical aspects to improve accuracy, such as incorporating a collision detection system between the nodes of the model. For further model validation, a parameter fitting method such as the method detailed in (Gobeawan et al., 2021b) can be applied.

Beyond the context of plant modeling, we note that our work in combining L-Systems, MSS and RBD could also have applications in modeling other objects such as bones and soft tissues (Golec, 2018), medical procedures (Nakao and Minato, 2010) and sound (Cahill, 2009).

ACKNOWLEDGEMENTS

This research/project is supported by the National Research Foundation, Singapore under its Industry Alignment Fund – Pre-positioning (IAF-PP) Funding Initiative. Any opinions, findings and conclusions or recommendations expressed in this material are those of the authors and do not reflect the views of National Research Foundation, Singapore.

REFERENCES

- Alani, A. M. and Lantini, L. (2020). Recent advances in tree root mapping and assessment using non-destructive testing methods: a focus on ground penetrating radar. *Surveys in Geophysics*, 41:605–646.
- Atkinson, J. A., Pound, M. P., Bennett, M. J., and Wells, D. M. (2019). Uncovering the hidden half of plants using new advances in root phenotyping. *Current opinion in biotechnology*, 55:1–8.
- Balouch, Z., Hajji, R., Poux, F., Kharroubi, A., and Billen, R. (2022). A prior level fusion approach for the semantic segmentation of 3d point clouds using deep learning. *Remote Sensing*, 14(14):3415.
- Baraff, D. (2001). Physically based modeling: Rigid body simulation. *SIGGRAPH Course Notes, ACM SIGGRAPH*, 2(1):2–1.
- Betsch, P. and Siebert, R. (2009). Rigid body dynamics in terms of quaternions: Hamiltonian formulation and conserving numerical integration. *International journal for numerical methods in engineering*, 79(4):444–473.
- Boudon, F., Pradal, C., Cokelaer, T., Prusinkiewicz, P., and Godin, C. (2012). L-py: an l-system simulation framework for modeling plant architecture development based on a dynamic language. *Frontiers in plant science*, 3:76.
- Cahill, B. (2009). Physically based sound synthesis for interactive applications. *Master's thesis, University of Dublin, Trinity College*.
- Dumais, J. (2013). Beyond the sine law of plant gravitropism. *Proceedings of the National Academy of Sciences*, 110(2):391–392.

- Gobeawan, L., Lin, E., Tandon, A., Yee, A., Khoo, V., Teo, S., Yi, S., Lim, C., Wong, S., Wise, D., et al. (2018). Modeling trees for virtual singapore: From data acquisition to citygml models. *The International Archives of the Photogrammetry, Remote Sensing and Spatial Information Sciences*, 42:55–62.
- Gobeawan, L., Lin, S., Liu, X., Wong, S., Lim, C., Gaw, Y., Wong, N., Tan, P., Tan, C., and He, Y. (2021a). Ifc-centric vegetation modelling for bim. *ISPRS Annals of the Photogrammetry, Remote Sensing and Spatial Information Sciences*, 8:91–98.
- Gobeawan, L., Wise, D. J., Wong, S. T., Yee, A. T., Lim, C. W., and Su, Y. (2021b). Tree species modelling for digital twin cities. *Transactions on Computational Science XXXVIII*, pages 17–35.
- Golec, K. (2018). *Hybrid 3D mass spring system for soft tissue simulation*. PhD thesis, Université de Lyon.
- Hädrich, T., Benes, B., Deussen, O., and Pirk, S. (2017). Interactive modeling and authoring of climbing plants. In *Computer Graphics Forum*, volume 36, pages 49–61. Wiley Online Library.
- Harahap, N., Siregar, I., and Dwiyantri, F. (2018). Root architecture and its relation with the growth characteristics of three planted shorea species (dipterocarpaceae). In *IOP Conference Series: Earth and Environmental Science*, volume 203, page 012016. IOP Publishing.
- Imhoff, S., Pires da Silva, A., Ghiberto, P. J., Tormena, C. A., Pilatti, M. A., and Libardi, P. L. (2016). Physical quality indicators and mechanical behavior of agricultural soils of argentina. *PLoS One*, 11(4):e0153827.
- Jirasek, C., Prusinkiewicz, P., and Moulia, B. (2000). Integrating biomechanics into developmental plant models expressed using l-systems. *Plant biomechanics*, pages 615–624.
- Kang, Y.-M., Choi, J.-H., Cho, H.-G., and Lee, D.-H. (2001). An efficient animation of wrinkled cloth with approximate implicit integration. *The Visual Computer*, 17:147–157.
- Kang, Y.-M., Choi, J.-H., Cho, H.-G., and Park, C.-J. (2000). Fast and stable animation of cloth with an approximated implicit method. In *Proceedings Computer Graphics International 2000*, pages 247–255. IEEE.
- Lim, S. M. and Gobeawan, L. (2023). Hybrid mass-spring l-system for modelling tree interactions with environment. In Chen, T.-W. C., Fricke, A., Kahlen, K., and Stützel, H., editors, *Book of Abstracts of the 10th International Conference on Functional-Structural Plant Models: FSPM2023, 27- 31 March 2023*, pages 102–103.
- Mesit, J., Guha, R. K., and Chaudhry, S. (2007). 3d soft body simulation using mass-spring system with internal pressure force and simplified implicit integration. *J. Comput.*, 2(8):34–43.
- Moulton, D. E., Oliveri, H., and Goriely, A. (2020). Multiscale integration of environmental stimuli in plant tropism produces complex behaviors. *Proceedings of the National Academy of Sciences*, 117(51):32226–32237.
- Nakao, M. and Minato, K. (2010). Physics-based interactive volume manipulation for sharing surgical process. *IEEE Transactions on Information Technology in Biomedicine*, 14(3):809–816.
- Pang, J., Lin, X., Zhang, X., Ji, J., and Geng, L. (2023). Modelling and analysis of penetration resistance of probes in cultivated soils. *PLoS one*, 18(1):e0280525.
- Pedersen, S. W. (2003). Simulation of rigid body dynamics. Master's thesis.
- Pomeroy, J. (2023). *Hardware, Software, Heartware: Digital Twinning for More Sustainable Built Environments*. Taylor & Francis.
- Prusinkiewicz, P. and Lindenmayer, A. (1990). *The Algorithm Beauty of Plants*. Springer.
- Rezaur, R., Rahardjo, H., Leong, E., and Lee, T. (2003). Hydrologic behavior of residual soil slopes in singapore. *Journal of Hydrologic Engineering*, 8(3):133–144.
- Russell, D. and Hunt, L. (2009). Spring constants for hockey sticks. *The Physics Teacher (submitted draft)*. Retrieved from: www.acs.psu.edu/drussell/publications/russell-hunt-tpt-formatted.pdf (Accessed 17 January 2014).
- Smith, J. O. (2010). *Physical audio signal processing: For virtual musical instruments and audio effects*. W3K Publishing.
- Stava, O., Pirk, S., Kratt, J., Chen, B., Měch, R., Deussen, O., and Benes, B. (2014). Inverse procedural modelling of trees. In *Computer Graphics Forum*, volume 33, pages 118–131. Wiley Online Library.
- Suzuki, T. and Arikawa, T. (2010). Numerical analysis of bulk drag coefficient in dense vegetation by immersed boundary method. In *Proc. of the 32nd Conference on Coastal Engineering*.
- Tao, F., Xiao, B., Qi, Q., Cheng, J., and Ji, P. (2022). Digital twin modeling. *Journal of Manufacturing Systems*, 64:372–389.
- Van Haevre, W., Di Fiore, F., and Van Reeth, F. (2006). Physically-based driven tree animations. In *NPH*, pages 75–82.
- Witkin, A., Baraff, D., and Kass, M. (2001). Physically based modeling. *ACM SIGGRAPH Course Notes*, 25.
- Wong, N. H., Tan, C. L., Kolokotsa, D. D., and Takebayashi, H. (2021). Greenery as a mitigation and adaptation strategy to urban heat. *Nature Reviews Earth & Environment*, 2(3):166–181.
- Yi, L., Li, H., Guo, J., Deussen, O., and Zhang, X. (2018). Tree growth modelling constrained by growth equations. In *Computer Graphics Forum*, volume 37, pages 239–253. Wiley Online Library.
- Zhou, Y., Wang, Y., Chen, X., Zhang, L., and Wu, K. (2017). A novel path planning algorithm based on plant growth mechanism. *Soft Computing*, 21:435–445.